JOURNAL OF APPLIED ELECTROCHEMISTRY 9 (1979) 369–379

Impedance parameters and the state-of-charge. II. Lead-acid battery

M. L. GOPIKANTH, S. SATHYANARAYANA

Department of Inorganic and Physical Chemistry, Indian Institute of Science, Bangalore 560 012, India

Received 8 June 1978

The determination of the state-of-charge of the lead–acid battery has been examined from the viewpoint of internal impedance. It is shown that the impedance is controlled by charge transfer and to a smaller extent by diffusion processes in the frequency range 15–100 Hz. The equivalent series/parallel capacitance as well as the a.c. phase-shift show a parabolic dependence upon the state-of-charge, with a maximum or minimum at 50% charge. These results are explained on the basis of a uniform transmission-line analog equivalent circuit for the battery electrodes.

Nomenclature

Battery This word is used synonymous with the word 'cell'
R_p equivalent parallel resistance (Ω)
R_s equivalent series resistance (Ω)
$|Z|$ modulus of impedance (Ω)
C_p equivalent parallel capacitance (F)
C_s equivalent series capacitance (F)
ϕ a.c. phase-shift (radians or degrees)
ω $2\pi f$
f a.c. frequency (Hz)
R_Ω resistance of electrolyte solution and separator (Ω)
$\bar{C}$ double layer capacity (F)
W diffusional (Warburg) impedance (Ω)
R_t resistance due to polarization (Ω)
α energy transfer coefficient
T absolute temperature (K)
R gas constant
F Faraday constant
C_O^0 bulk concentration of the oxidant
C_R^0 bulk concentration of the reductant
D_O diffusion coefficient of the oxidant
D_R diffusion coefficient of the reductant
σ Warburg coefficient
N number of pores/area
A active area of the electrode (cm^2)
S state-of-charge
a anode
c cathode
L inductance
I_o exchange current

1. Introduction

The state-of-charge of a battery refers to the ratio of residual capacity at a given instant to the maximum capacity available from the battery. A knowledge of the state-of-charge not only helps in predicting the residual capacity, but also helps in increasing the cycle life of the battery by proper control on the degree of charge and the depth of discharge in each cycle.

Various methods used in the literature to determine the state-of-charge of different systems have been summarized in part I of this series [1].

In the present work, the problem of non-destructive determination of the state-of-charge (S) of the lead–acid battery has been re-examined. Due to the fact that ions of the electrolyte solution or molecules of the solvent take part in the electrode reactions of a battery, it may be anticipated that the density of the solution in a battery may change with the state-of-charge. Such a situation indeed prevails with the conventional lead–acid battery where, the overall reaction is

$$Pb + PbO_2 + 2H_2SO_4 \rightleftarrows 2PbSO_4 + 2H_2O \quad (1)$$

According to Equation 1, the density of the solution should decrease on discharge since one

mole of water is produced for every mole of sulphuric acid consumed during discharge. The usual vented lead–acid batteries with flooded electrolyte show a change in the density of solution from* about $1{\cdot}3\,g\,ml^{-1}$ at $S = 0{\cdot}9$ to about $1{\cdot}2\,g\,ml^{-1}$ at $S = 0{\cdot}1$. Since hydrometers can easily be constructed to read density to an accuracy of $\pm\ 0{\cdot}005$, it is possible to predict the state-of-charge within about 10% over the useful portion of the discharge curve.

The method is unfortunately not of general applicability in the case of lead–acid batteries, since the modern trend is to develop batteries with gelled electrolytes or a hermetically sealed unit which precludes the use of density measurements to predict the state-of-charge.

Since the open-circuit voltage (OCV) at equilibrium is equal to the e.m.f. of a battery, it may be expected that this depends on the effective activity of the reactants and therefore on the state-of-charge. However, difficulties arise due to significant battery-to-battery variations in e.m.f. at the same state-of-charge which occur because of variable crystallographic forms and degree of nonstoichiometry of the PbO_2 and $PbSO_4$ active materials at the electrodes. Such physical changes in electrode materials of a given chemical type are known to cause differences in equilibrium electrode potentials of several tens of mV†. If it is assumed that such variations in electrode potentials of the positive and negative electrodes reinforce each other (worst case), it may be concluded that battery-to-battery variations in e.m.f. at a given state-of-charge may be of the order of 50 mV due to variations in manufacturing processes, ageing and charge–discharge cycling.

Hence, a prediction of the state-of-charge from equilibrium values of open-circuit voltage is likely to be successful only if the change in equilibrium OCV is of the order of 500 mV between a state-of-charge 0·1–0·9. Since experiments show that the change in the OCV of a lead–acid battery at equilibrium is from about 2·25 V at 0·9 state-of-charge to about 1·95 V at 0·1 state-of-charge, the equilibrium OCV criterion only predicts the state-of-charge poorly.

It was shown in part I of this series [1] that it is possible to get an indication of the state-of-charge of a sintered-plate nickel–cadmium battery by measurement of equivalent series/parallel capacitance or of phase-shift at a sufficiently low alternating current test frequency.

In the present work, the problem of non-destructive determination of the state-of-charge of the lead–acid battery has been explored similarly by measurement of impedance parameters and the results interpreted theoretically using an idealized model for the porous electrodes of the battery.

2. Experimental

2.1. *Cells*

The lead–acid cells used were of gelled-electrolyte maintenance-free design (7·5 Ah nominal capacity) manufactured by Sonnenshein (Germany). The cells were subjected to three 'conditioning' cycles of charge–discharge and their capacities matched to within 5%. Two such cells were used for the tests.

2.2. *Procedure*

The cells were subjected to one deep charge–discharge cycle before the test began. This has the effect of activating the surfaces of the electrodes and making their performance reproducible. It was found during preliminary experiments that when cells are charged (or discharged) several hours are required for the open-circuit voltage to become constant i.e., to re-establish equilibrium.

Cells at different states-of-charge were obtained as follows. Since the absolute capacity was known by earlier charge–discharge studies, a pre-determined amount of charge was withdrawn by discharge at constant current (or introduced by charging at constant current) at the ten-hour rate ($C/10$). A ten-hour rest period was then allowed before the measurements were begun.

2.3. *Set-up*

Impedance parameters were measured using the

* The actual values vary to some extent depending on the volume of the solution in a battery of a given capacity.

† For example, the reversible potential of zinc in contact with KOH solution saturated with zincate ions has been shown [6] to vary about 20 mV depending on the solid phase (α-$Zn(OH)_2$, γ-$Zn(OH)_2$, ϵ-$Zn(OH)_2$ or ZnO) in equilibrium with the solution.

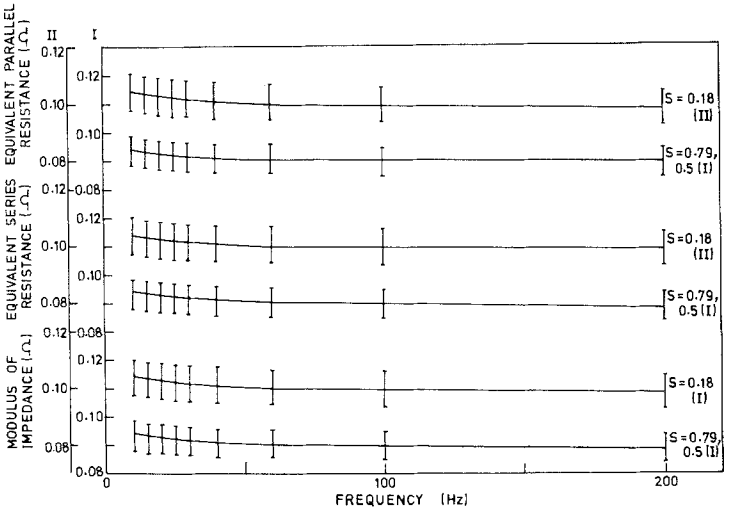

Fig. 1. Dependence of equivalent parallel resistance (R_p), equivalent series resistance (R_s) and modulus of impedance ($|Z|$) of lead–acid cell on a.c. frequency at different states-of-charge.

a.c. bridge method. Since a charged lead–acid cell is a direct-current power source, modifications are necessary in the design of the a.c. bridge. The details of the method adopted to obtain equivalent series (or parallel) resistance $R_s(R_p)$, equivalent series (or parallel) capacitance $C_s(C_p)$ and a.c. phase-shift ϕ are described in part I of the present series [1].

3. Results

At a.c. frequencies above 200 Hz, the inductive reactance of the cells became prominent as indicated by the tendency of C_p to become negative at the balance point. This is probably due to the porous structure of (especially the negative) the electrodes. Since the inductive and capacitive components of the cell could not be separated, the impedance measurements were restricted to a.c. frequencies below 100 Hz. The lowest frequency that could be used was governed by the available range of C_p in the balancing arm, since, as the a.c. frequency is decreased the required value of C_p sharply increases below 10 Hz. Thus the range adopted was 10–100 Hz.

The results obtained for the equivalent series resistance (R_s), equivalent parallel resistance (R_p) and modulus of impedance ($|Z|$) as a function of a.c. frequency at different states-of-charge are shown in Fig. 1. It is seen that there is no signifi-

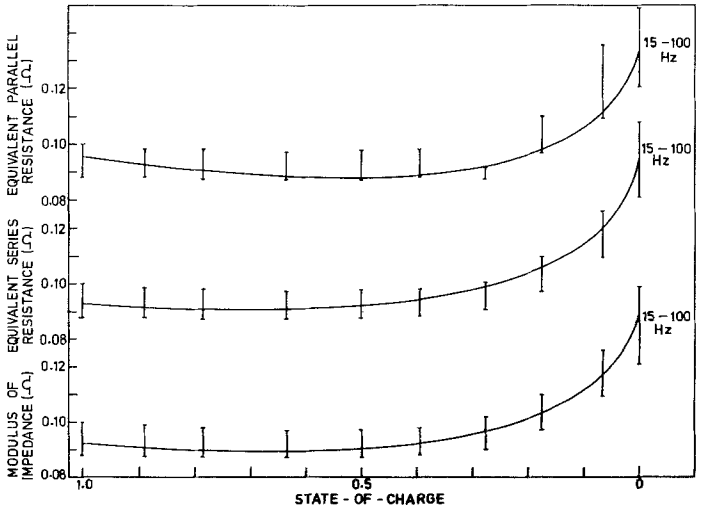

Fig. 2. Dependence of equivalent parallel resistance (R_p), equivalent series resistance (R_s) and modulus of impedance ($|Z|$) on state-of-charge of lead–acid cell at different frequencies (15–100 Hz).

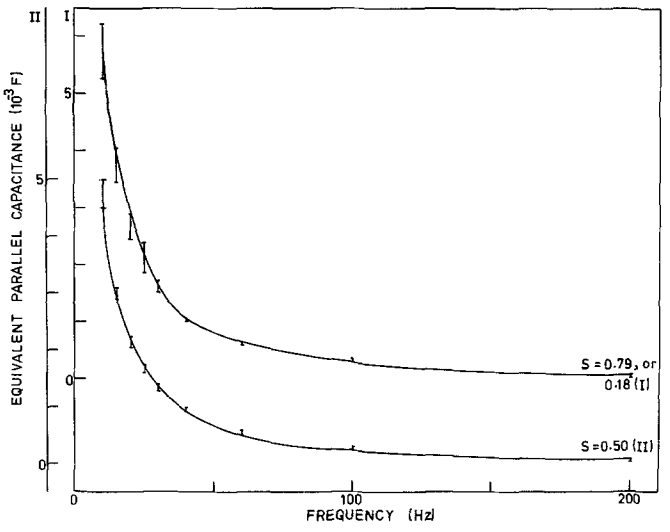

Fig. 3. Dependence of equivalent parallel capacitance (C_p) on a.c. frequency at different states-of-charge for lead–acid cell.

cant variation of the parameters with an increase in frequency.

The dependence of R_p, R_s and $|Z|$ on the state-of-charge of the lead–acid cells at different a.c. frequencies are shown in Fig. 2. All the parameters show a slight increase in their values towards the end of discharge and are independent of a.c. frequency in the range 15–100 Hz.

The variation of equivalent series capacitance (C_s) and equivalent parallel capacitance (C_p) with a.c. frequency (Figs. 3 and 4) at two different states-of-charge show that in all the cases there is initially a steep fall in their values. Thereafter (above 50 Hz) the values remain constant.

The equivalent series capacitance (C_s) and equivalent parallel capacitance (C_p) behave differently from each other with a variation in the state-of-charge at constant a.c. frequency. At about 0·5 state-of-charge, C_p shows a flat minimum (Fig. 5), and C_s shows a broad maximum (Fig. 6). The phase angle between alternating cell current and cell voltage varies with a.c. frequency as shown in Fig. 7. If the frequency is held constant there is an approximately parabolic variation of phase-shift ϕ with the state-of-charge (Fig. 8) with a minimum at $S \approx 0{\cdot}5$.

4. Discussion

As a circuit element, a galvanic cell (or a battery)

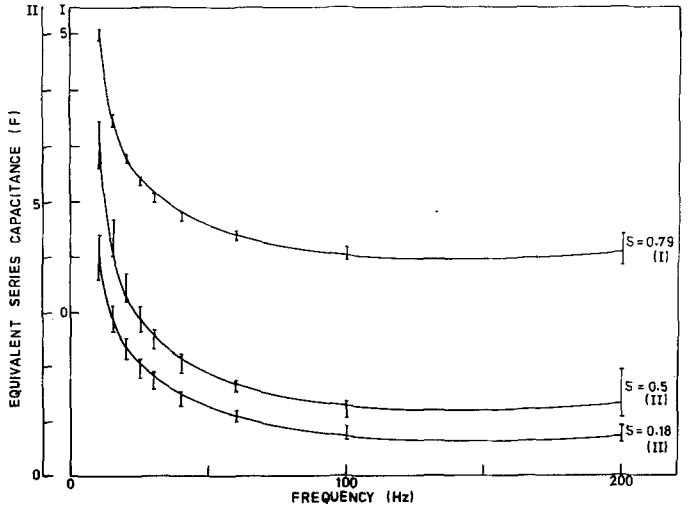

Fig. 4. Dependence of equivalent series capacitance (C_s) on a.c. frequency of lead–acid cell at different states-of-charge.

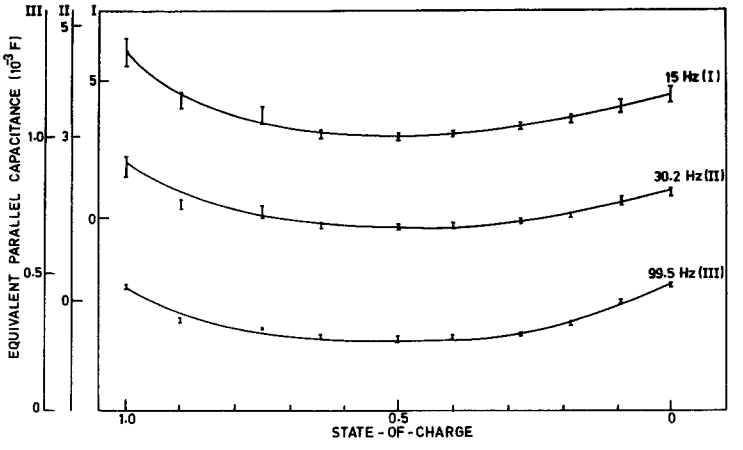

Fig. 5. Dependence of equivalent parallel capacitance (C_p) on state-of-charge of lead–acid cell at different frequencies.

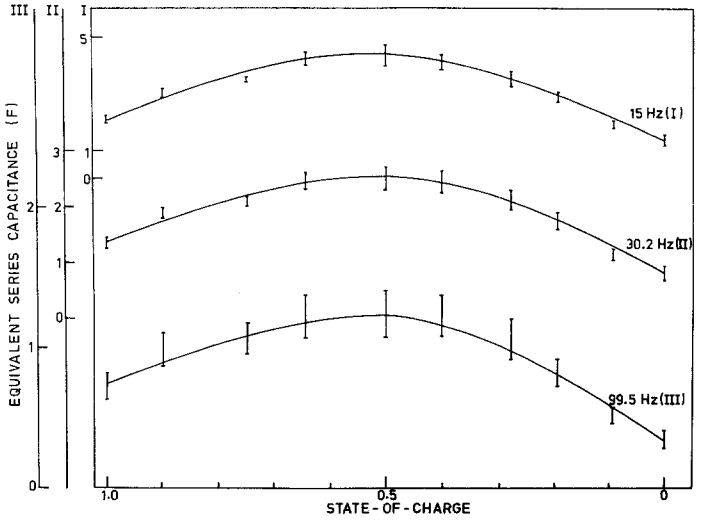

Fig. 6. Dependence of equivalent series capacitance (C_s) on state-of-charge of lead–acid cell at different frequencies.

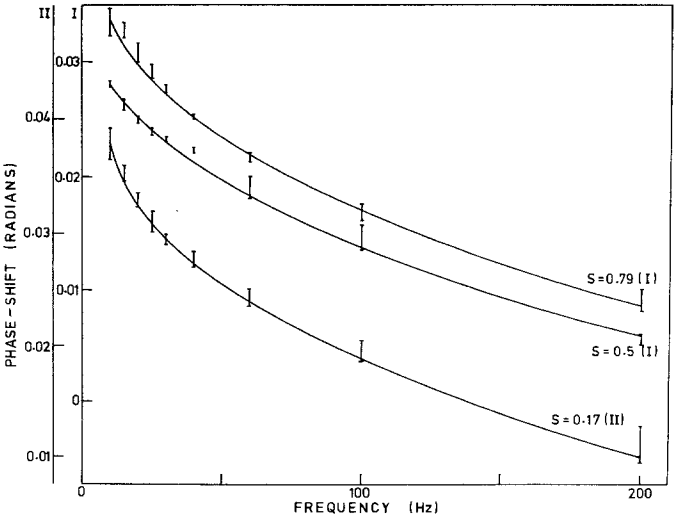

Fig. 7. Dependence of phase-shift (ϕ) of lead–acid cell on a.c. frequency at different states-of-charge.

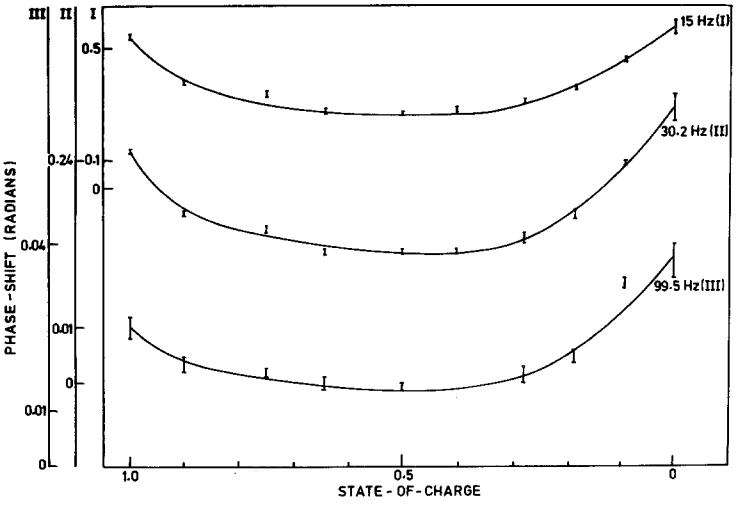

Fig. 8. Dependence of phase-shift (ϕ) on state-of-charge of lead–acid cell at different frequencies.

may always be represented [2], as an ideal voltage source (i.e., without any internal impedance) in series with a combination of a reactance (usually capacitive) and a resistance in either a parallel mode (R_p–C_p) or a series mode (R_s–C_s) as shown in Fig. 9.

From circuit theory, it follows that the complex impedance of the cell is given by

$$Z = R_s + \frac{1}{j\omega C_s} = \frac{R_p}{(1 + j\omega C_p R_p)} \qquad (2)$$

where $\omega = 2\pi f$, f being the frequency (Hz). The impedance of each electrode of a cell in a battery will have contributions from charge and mass transfer processes as well as from the double layer capacitance and lead inductance. The electrolyte solution and separator will contribute a resistance to the battery impedance. Finally, the battery electrodes will contribute a 'geometrical' capacitance due to their close parallel spacing. Taking into account the above facts and following the classical Randles' equivalent circuit for single electrodes [3], the equivalent circuit of a galvanic cell may be represented as follows (Fig. 10).

The following assumptions are made to simplify further analysis. Since the two electrodes of the battery behave similarly their electrode impedances may be combined to give a single impedance consisting of new, effective values of double layer capacitance ($\bar{C}$), charge transfer resistance (R_t) and mass transfer impedance (W) of the battery interconnected as for a single electrode. The actual expressions for these are unimportant for the present discussion.

By choosing a sufficiently low a.c. frequency for impedance measurements, it is possible to ensure, as shown in Section 3, that the inductive reactance is small compared to the capacitive reactance i.e., L_a, L_c may be neglected in Fig. 10.

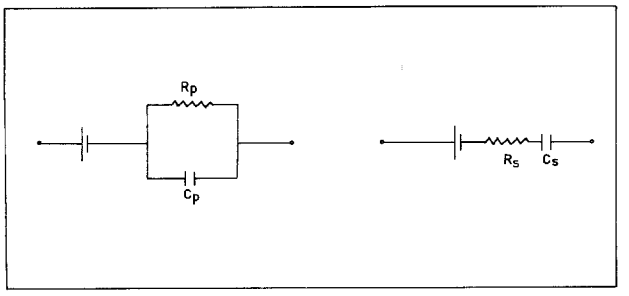

Rp = Equivalent parallel resistance
Rs = Equivalent series resistance
Cp = Equivalent parallel capacitance
Cs = Equivalent series capacitance

Fig. 9. Lumped equivalent circuit of a cell as a circuit element.

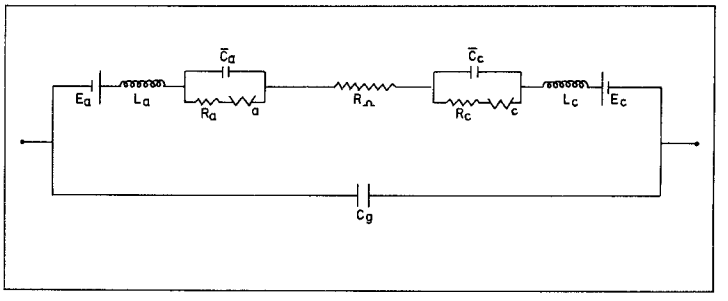

Ea, Ec = Single electrode potentials
La, Lc = Lead inductances
Ca, Cc = Double layer capacitances
Ra Rc = Charge transfer resistances

Wa Wc = Diffusional (Warburg) impedance
Rn = Resistance of solution and separator
Cg = Interelectrode capacitance

Subscript a, c denote anode and cathode respectively

Fig. 10. Equivalent circuit of a battery or cell.

For practical battery systems, the geometrical capacitance is smaller than the measured capacitance by several orders, C_g may therefore be omitted from Fig. 10.

Thus the modified equivalent circuit of a battery may be represented as shown in Fig. 11, i.e., again a typical Randles' equivalent circuit. The limiting forms of the impedance parameters of the Randles' equivalent circuit have been thoroughly reviewed in the literature [1, 3]. In particular these show that a plot of $(1/\omega C_s)$ versus R_s is a straight line or a semi-circle depending on either a predominantly diffusion-control or charge-transfer control of the impedance.

The $(1/\omega C_s)$ versus R_s plots for the lead–acid cell at different states-of-charge are shown in Figs. 12 and 13. The plots suggest the form of a semi-circle but somewhat drawn out towards the low frequency end. It is therefore likely that there is major control by charge transfer polarization modified by some diffusion polarization.

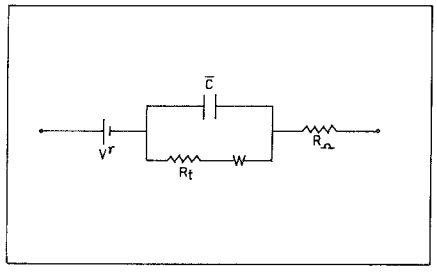

Vr = Ec – Ea = EMF of the battery
Rt = Charge tranfer resistance
W = Diffusional (Warburg) impedance
C = Double layer capacitance
Rn = Resistance of solution and separator

Fig. 11. Equivalent circuit of a battery (simplified).

If we approximate the plots in Figs. 12 and 13 as parts of a semi-circle i.e., as mainly controlled by charge transfer [7], it follows from the analysis of Randles' circuit (Equations 16–18 of [1]) that

$$C_s \approx \bar{C} + 1/(\omega^2 \bar{C} R_t^2) \qquad (3)$$

i.e., C_s versus $(1/\omega^2)$ should be a straight line with a positive intercept. Correspondingly Figs. 14–16 show that a well-defined straight line is not obtained.

Since the lead–acid cell consists of porous electrodes, it may be possible to improve the model by introducing the essential elements of porous electrode behaviour into the Randles' equivalent circuit. Since the geometry of the porous electrode defies a complete description at the present time, we may assume the simplest reasonable model as that of the porous electrodes being comprised of a large number of uniform, long cylindrical tubes filled with the active material.

In this model, the electrical analogue of each 'pore' of the porous electrode is a distributed impedance of a uniform transmission-line type as characterized in Fig. 17. If the ratio of pore length to pore diameter is large compared to unity, which is quite realistic in the case of lead–acid cell electrodes, the complex impedance of the active material-flooded porous tube is obtained from transmission-line theory as,

$$Z_0 = (Z_1 Z_2)^{1/2} \qquad (4)$$

It may be noted that R_Ω is outside the porous electrode structure and, therefore, not a part of

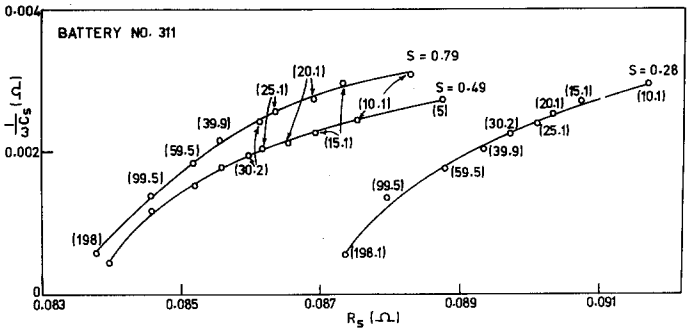

Fig. 12. Argand plot of lead–acid cell at different states-of-charge (S = state-of-charge). The numbers on curves indicate the a.c. frequency (Hz).

the distributed electrode impedance. It is also assumed that the electrode impedances of the anode and cathode are additive which is quite reasonable since they are not coupled in any other way.

Since diffusion is coupled to charge-transfer control as shown in Figs. 12 and 13, the impedance Z_1 is characterized for diffusion as

$$Z_1 = (\sigma_1/\sqrt{\omega}) - j(\sigma_1/\sqrt{\omega}) \qquad (5)$$

where σ_1 is defined according to the following equation, for the species diffusing along the axis of the pore.

$$\sigma_1 = \frac{RT}{n^2F^2A\sqrt{(2\omega)}}\left(\frac{1}{C_O^0\sqrt{D_O}} + \frac{1}{C_R^0\sqrt{D_R}}\right) \qquad (6)$$

Such an expression for σ_1 is reasonable because the cell impedance is measured under near-equilibrium conditions (no d.c. polarization). No terms due to polarization resistance or double layer capacitance are introduced in Z_1 because diffusion of species along the long axis of the pore is not directly associated with charge transfer or double layer formation. The complex impedance Z_2, however, is bound to be different since the charge transfer polarization is shown by experiment to be important. As a first approximation therefore we may ignore any diffusional impedance in Z_2 but retain the charge transfer polarization resistance shunted by the double layer capacitance as in Fig. 18. Hence

$$Z_2 = \frac{1}{(1/R_t) + j\omega\bar{C}} = \frac{R_t - j\omega\bar{C}R_t^2}{1 + \omega^2\bar{C}^2R_t^2} \qquad (7)$$

and from Equations 4, 5 and 7, it follows

$$Z_0 = \left\{\frac{\sigma_1}{\sqrt{\omega}}(1-j) \times \left[\frac{R_t}{1+\omega^2\bar{C}^2R_t^2}(1 - j\omega\bar{C}R_t)\right]\right\}^{1/2}. \qquad (8)$$

The resistive and reactive parts of Equation 8 may be separated*

$$|Z| = \left[R_s^2 + \frac{1}{\omega^2C_s^2}\right]^{1/2} \qquad (9)$$

* Only the reactive part is of interest to us since the resistive part is additive to the much larger term R_Ω (Equation 10) in the battery impedance, and is therefore insensitive to state-of-charge variations.

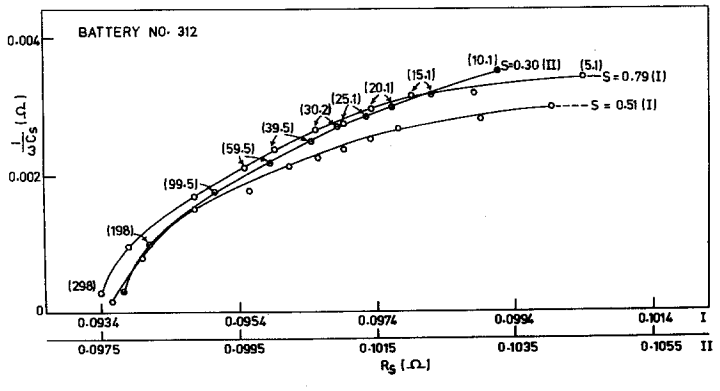

Fig. 13. Argand plot of lead–acid cell at different states-of-charge (S = state-of-charge). The numbers on curves indicate the a.c. frequency (Hz).

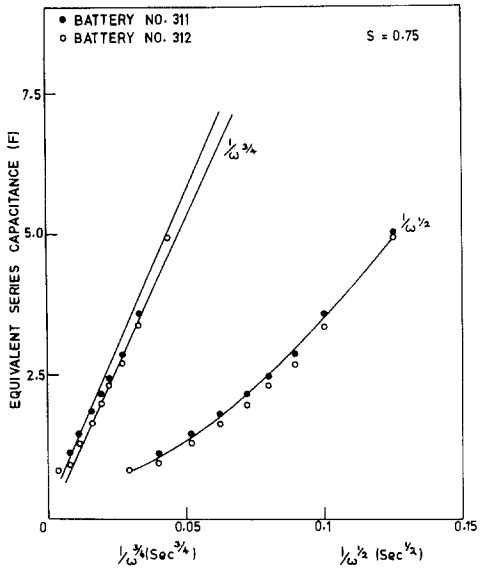

Fig. 14. Dependence of equivalent series capacitance (C_s) on $(1/\omega^{1/2})$ and on $(1/\omega^{3/4})$ of lead–acid battery (S = state-of-charge).

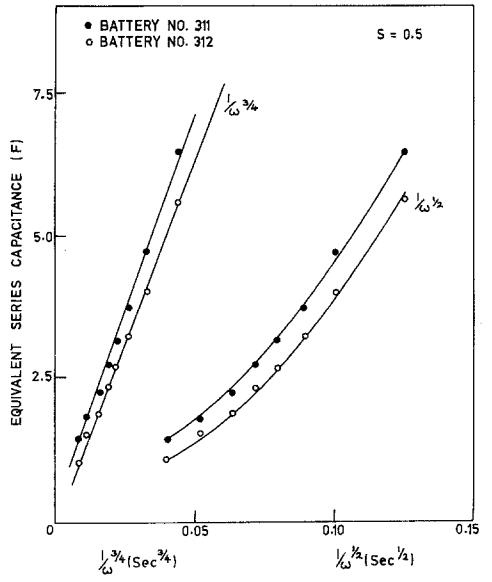

Fig. 15. Dependence of equivalent series capacitance (C_s) on $(1/\omega^{1/2})$ and on $(1/\omega^{3/4})$ of lead–acid battery (S = state-of-charge).

$$NAR_s = R_\Omega + \left\{\frac{\sigma_1 R_t[\sqrt{(2 + 2\omega^2\bar{C}^2R_t^2)} + (1 - \omega\bar{C}R_t)]}{2\sqrt{\omega}(1 + \omega^2\bar{C}^2R_t^2)}\right\}^{1/2} \tag{10}$$

$$\frac{NA}{\omega C_s} = \left\{\frac{\sigma_1 R_t[\sqrt{(2 + 2\omega^2\bar{C}^2R_t^2)} - (1 - \omega\bar{C}R_t)]}{2\sqrt{\omega}(1 + \omega^2\bar{C}^2R_t^2)}\right\}^{1/2} \tag{11}$$

where N is the number of cylindrical pores per unit area of the electrode, and A the area of the electrode.

Assuming that $\omega\bar{C}R_t \ll 1$ (which is justified in this case), Equations 10 and 11 may be simplified to give

$$NAR_s = R_\Omega + \left[\frac{\sigma_1 R_t(\sqrt{2} + 1)}{2\sqrt{\omega}}\right]^{1/2} \tag{12}$$

$$NA(1/\omega C_s) = \left[\frac{\sigma_1 R_t(\sqrt{2} - 1)}{2\sqrt{\omega}}\right]^{1/2}. \tag{13}$$

According to Equation 13, a plot of C_s versus $(1/\omega^{3/4})$ should be a straight line passing through the origin. Such a plot constructed from experimental data is shown in Figs. 14–16 at different states-of-charge of the battery. It may be seen from the figures that there is a good agreement with the theory.

Thus, the model proposed may be considered to be realistic for the lead–acid battery system.

The equivalent circuit for a single pore in the electrodes of the battery or cell impedance can therefore be represented as in Fig. 19.

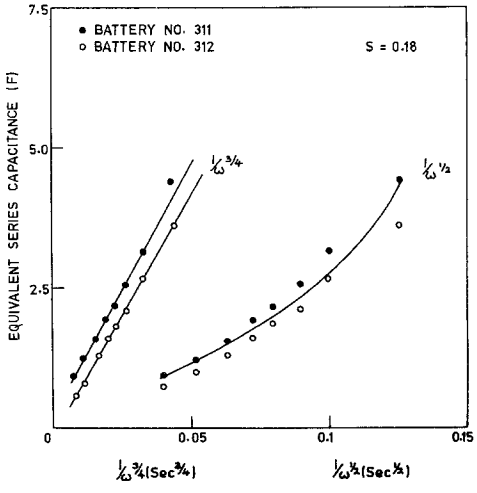

Fig. 16. Dependence of equivalent series capacitance (C_s) on $(1/\omega^{1/2})$ and on $(1/\omega^{3/4})$ of lead–acid battery (S = state-of-charge).

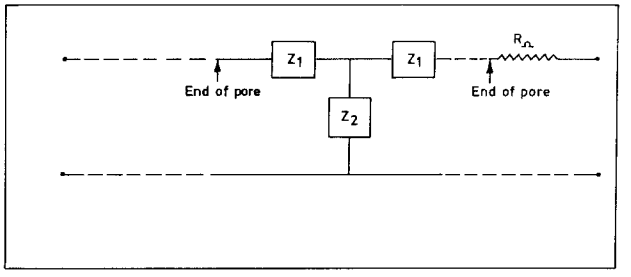

Fig. 17. Transmission-line model of a single pore in the porous electrodes of a battery or cell.

The solution resistance R_Ω is a dominant term in $|Z|$, R_s and R_p. Hence inevitable fluctuations in R_Ω will mask any change of the above parameters with the state-of-charge of the cell. Thus, $|Z|$, R_s or R_p cannot be used as state-of-charge indicator. On the other hand C_s, C_p or ϕ show a somewhat parabolic dependence on the state-of-charge. On the basis of the model proposed above these facts may be explained as follows.

The charge transfer resistance R_t is related to an effective exchange current I_0 of the electrode reactions by an equation of the form

$$R_t = \frac{RT}{nFI_0}. \tag{14}$$

Assuming a homogeneous solid solution of the reacting species at each battery electrode, it may be shown that [4, 5] approximately*

$$I_0 \propto [S(1-S)]^{1/2}. \tag{15}$$

It therefore follows that

$$R_t = k\left\{\frac{1}{[S(1-S)]^{1/2}}\right\} \tag{16}$$

where k is a constant. From Equations 13 and 16

$$C_s = h'\left\{\frac{[S(1-S)]^{1/2}}{\omega^{3/2}}\right\}^{1/2} \tag{17}$$

where h' is a constant. Hence, at a given alternating-current frequency, C_s versus S should have a maximum at $S = 0{\cdot}5$ and the curve should tend to zero at $S = 0$ and $S = 0{\cdot}9$. These results are in full agreement with experiment (Fig. 6).

The phase-shift ϕ is related to C_s by circuit theory as $\cot\phi = \omega C_s R_s$. Since it has been found by experiment that $\phi \ll 1$, and $R_s \approx R_\Omega$

$$\phi \approx \frac{1}{\omega C_s R_s} \approx \frac{1}{\omega C_s R_\Omega}. \tag{18}$$

From Equations 13 and 14

$$\phi = \frac{1}{h'' R_\Omega [S(1-S)\omega]^{1/4}} \tag{19}$$

where h'' is a constant.

Hence, at a given alternating-current frequency the phase-shift should show a minimum at $S = 0{\cdot}5$ and increase indefinitely near the extremes $S = 0$ and $1{\cdot}0$. Experimental data are in qualitative agreement with these results (Figs. 5 and 8). The fact that ϕ does not show an indefinite increase at $S = 0$ and $S = 1{\cdot}0$ in Fig. 8 is explained by noting that in the usual experiments a battery that is allowed to rest for a few hours to attain equilibrium after a full charge always gets discharged slightly by self-discharge leading to $S < 1$.

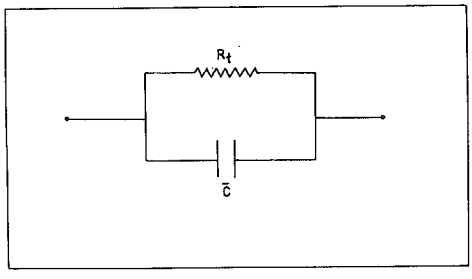

R_t = Charge transfer resistance
C = Double layer capacitance

Fig. 18. Model of the equivalent circuit for the impedance Z_2 in Fig. 17 in the case of lead–acid cell or battery.

* We have $I_0 \propto C_0^{(1-\alpha)} C_R^{\alpha}$, where α is the transfer coefficient. For a homogeneous solid solution, $C_0 \propto (Q^0 - Q)$, $C_R \propto Q$: also $\alpha \approx 0{\cdot}5$, and $S = (Q^0 - Q)/Q^0$. On substituting these in Equation 14, Equation 15 results.

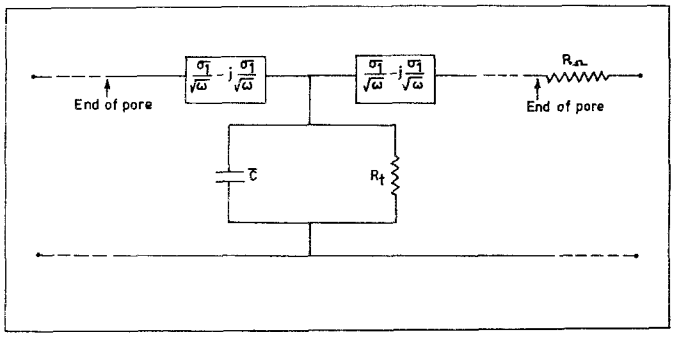

σ_1 = Warburg coefficient
$\bar{C}$ = Double layer capacitance, $j = \sqrt{-1}$
R_Ω = Resistance of solution and separator
$\omega = 2\pi f$, f = frequency (Hz)
R_t = Charge transfer resistance

Fig. 19. Transmission-line model for the equivalent circuit of a single pore in the electrodes of a lead–acid cell.

Similarly a battery discharged to 0 V and allowed to rest for a few hours (to attain equilibrium) regains some charge by a spontaneous decay of internal polarization of the porous electrodes leading to $S > 0$.

The observed parabolic dependence of C_s and ϕ on the state-of-charge of the lead–acid cell is thus satisfactorily explained from a fundamental angle. Nevertheless, a practical use of these correlations to determine the state-of-charge is limited in scope because, in general a given value of C_s or ϕ corresponds to two states-of-charge and a unique answer is not obtained.

5. Conclusions

The low alternating-current impedance of a lead–acid cell or a battery is largely controlled by charge-transfer and to a small extent by diffusion in the frequency range 15–100 Hz.

The internal resistance is dominated mainly by the resistance of the solution and of the separator between the electrodes. Hence, this parameter is not useful to characterize the state-of-charge of the cell.

The equivalent series/parallel capacitance and alternating-current phase-shift show a parabolic dependence with the state-of-charge at all frequencies (15–100 Hz). The use of these parameters for state-of-charge indicators is rather limited. since each value of capacitance or a.c. phase-shift corresponds to two states-of-charge.

The impedance data obtained may be quantitatively interpreted using the model that the cell electrodes consist of long cylindrical pores in which diffusion of ions occurs along the axis of the pore, while charge transfer reaction occurs at the double layer at the interface between the pore wall and the active material.

The factor underlying the variation of the a.c. phase-shift as well as of the equivalent series/parallel capacitance with the state-of-charge of the lead–acid cell may be identified as due to the variation of the charge transfer resistance (or the exchange currents of the electrode reactions) caused by the depletion (accumulation) of the reactants (products).

References

[1] S. Sathyanarayana, S. Venugopalan and M. L. Gopikanth, *J. Appl. Electrochem.* 9 (1979) 125.
[2] S. Sathyanarayana, S. Venugopalan and M. L. Gopikanth, *J. Appl. Electrochem.* 8 (1978) 479.
[3] M. Sluyters-Rehbach and J. H. Sluyters, 'Electroanalytical Chemistry', (Edited by A. J. Bard) Vol. 8, Marcel Dekker Inc. (1971) p. 157.
[4] S. Sathyanarayana, *Trans. Soc. Adv. Electrochem. Sci. Tech.* 11 (1976) 19.
[5] *Idem*, unpublished work.
[6] B. E. Conway and P. L. Bourgault, *Canad. J. Chem.* 37 (1959) 292.
[7] *Idem, ibid* 40 (1962) 1690.
[8] R. de Levie, 'Advances in Electrochemistry and Electrochemical Engineering', (Edited by P. Delahay and C. W. Tobias) Vol. 6, Interscience (1967) p. 329.